IN-BEHIND PERFORMANCE OF AN ICE CLASSED PROPELLER IN MODEL AND SHIP-SCALE

JENNIE ANDERSSON[*], ROBERT GUSTAFSSON[†], RIKARD JOHANSSON[†] AND RICKARD E. BENSOW[*]

[*]Department of Mechanics and Maritime Sciences
Chalmers University of Technology
Chalmersplatsen 4, 412 96 Gothenburg, Sweden
e-mail: jennie.andersson@chalmers.se, rickard.bensow@chalmers.se

[†] Kongsberg Hydrodynamic Research Centre
Kongsberg Maritime Sweden AB
Varnumsleden 5, 681 91 Kristinehamn, Sweden
e-mail: robert.gustafsson@km.kongsberg.com, rikard.johansson@km.kongsberg.com

Key words: Hull-propulsion system interaction, Ice classed propeller, RANS

Abstract. A CFD study in both model and ship-scale is conducted to compare the in-behind performance of an ice classed to a conventional propeller. In ship-scale the performance degradation of the ice classed propeller in-behind is less than in open water. Through evaluation of the blades performance tangentially and radially in the wake it is observed that the ice classed blade is superior at very low load, the blunter profiles is less sensitive to negative angles of attack. Contrary, in model-scale a larger difference in performance is noted between the propellers in-behind than expected from open water performance. This is most probably related to differences in Reynolds number between model-scale open water and self-propulsion tests, the thicker profiles of the ice classed propeller makes it additionally punished by the low Reynolds numbers of the self-propulsion tests.

1 INTRODUCTION

In ship design, model-scale testing in towing tanks and associated scaling procedures [1] is still the main tool for performance prediction for final comparisons between suppliers and contractual agreements. A critical part of the scaling procedure, and hence important for the final power prediction of the vessel, is establishment of the propulsive factors, such as thrust deduction (t), relative rotative efficiency (η_R) and Taylor wake fraction (w_T). When comparing different propulsion systems based on model-scale tests, differences in the propulsive factors are often not well understood. This is at least partly a consequence of that the propulsive factors as such are difficult to grasp since they aggregate several hydrodynamic differences in single numbers without any possibilities to separate the flow features contributing to the differences. In addition to that, differences in performance due to inconsistent Reynolds numbers (Re) of open water

and self-propulsion test may also be incorporated in the propulsive factors and contribute to difficulties in understanding them, as for instance discussed by [2, 3].

In this study an ice classed propeller has been studied in comparison to a conventional one, a common situation when a first test is done with a stock propeller and a final evaluation is done with the design propeller. This is such a case where differences in the propulsive factors may not be fully understood. The objective is to better understand the differences in in-behind performance between these two propulsion systems in model-scale, as well as in ship-scale.

2 METHOD

The study is based on analysis of a twin-skeg 120 m research vessel, for which the propulsion system is equipped with an integrated rudder bulb-propeller hubcap system. Two very similar 5-bladed controllable pitch propellers, one conventional and one with ice class (Polar Class 5) are designed for the purpose of this study. These propellers have not been manufactured, and hence no model-test data for these propellers is available for validation. However, this vessel has been tested with other propellers and this study replicates those model tests in terms of scale-factor and Reynolds numbers in open water and self-propulsion. The model-scale factor is 1:20.93 and only one operating condition is considered, the design point of the vessel, V_S = 13 knots corresponding to 1.462 m/s in model-scale. In model-scale the testing conditions are replicated while in ship-scale optimal trial conditions are assumed, i.e. no apparent wind, incoming waves or currents.

2.1 Vessel and Propulsion System

The hull characteristics are provided in Table 1, the hull is shown in Figure 1, and the stern of the vessel including propeller and rudder in Figure 2. In the model-scale tests the hull can be considered hydraulically smooth apart from that turbulence was triggered using a 50 mm wide sandpaper-stripe with its front located $0.1L_{PP}$ (Length between perpendicular) downstream the forward perpendicular. In ship-scale a clean anti-fouling coated hull is assumed. The two propellers have a conventional, identical, radial load distribution, a ship-scale propeller diameter (D_P) of 4.5 m, a pitch to diameter ratio, $P/D_{r/R=0.7} = 1.014$, and expanded blade area ratio equal to 0.531.

Table 1: Main characteristics of hull

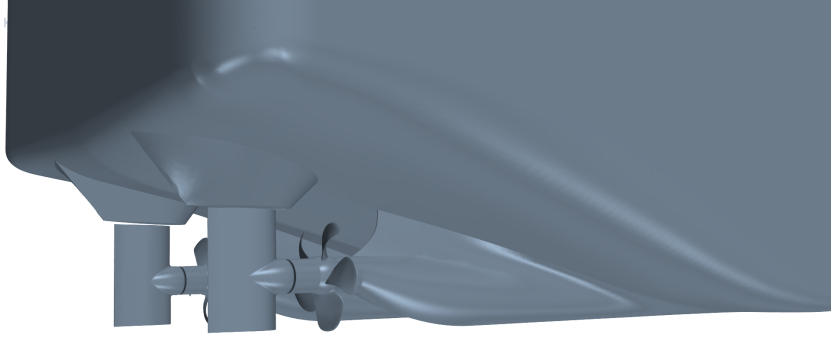|	Ship-scale	Model-scale
L_{PP} [m]	120.28	5.7468
Breadth [m]	24	1.1467
Total displacement [m^3]	15 201	1.6579
Block coefficient	0.7502	0.7502
Nominal draught [m]	7	0.334

2

Figure 1: Side-view of the hull

Figure 2: Aftship geometry

2.2 CFD Method

Computational Fluid Dynamics (CFD) using STAR-CCM+ ver. 2019.3 [4] is set up to try to replicate a full model-scale test and ship-scale operation, including fictive ship-scale open water and bare hull simulations. The conservation equations for momentum, mass, and turbulence quantities are solved using a segregated solver based on the SIMPLE algorithm. A second order upwind discretization scheme in space is used and a second order implicit scheme for time integration. Turbulence is modeled using SST $k - \omega$ [5, 6] with Quadratic constitutive relations (QCR) [7] and curvature correction [8, 4]. In model-scale, the laminar to turbulent transition is modelled using the $\gamma - Re_\theta$ transition model [9, 10] including the cross-flow term [11].

The propeller flow in open-water is solved using the steady RANS equations and utilizing multiple reference frames (MRF) with frozen rotor interfaces, where a rotating reference frame is specified for the propeller domain and a stationary reference frame for the outer domain. The propeller domain size is identical to the self-propulsion setup and the outer domain extends $6D_P$ upstream and downstream the propeller, with a diameter of $10D_P$. The advance velocity (V_A) is set on the inlet boundary to reach the desired advance ratios ($J = V_A/nD_P$). The propeller rotation rate (n) is set to 26 rps, in line with model tests for this vessel. In ship-scale it is set to 94.2 rpm, similar to the ship-scale self-propulsion rotation rate. The inlet turbulence intensity and turbulence viscosity ratio are set to 5 % and 10, respectively. In addition, for the model-scale setup, a turbulent kinetic energy source term is present upstream the propeller, to reduce the dissipation of turbulence from the inlet to the propeller. The resulting turbulence intensity just ahead of the propeller is about 2 %. On the outlet boundary, a static pressure is prescribed, while the far field lateral boundary is modeled as a symmetry plane.

The propulsion systems are compared using double-body models, however bare hull simula-

tions are carried out also with a free surface, to obtain the resistance to use for calculation of propulsive factors and to obtain an estimate for the resistance difference between a double-body and free-surface model. The size of the computational domain for the bare hull simulations, given in [x, y, z] where x is the longitudinal and z the vertical directions, is [-3.5L_{PP}:2.5L_{PP}, 0:2L_{PP}, -1.5L_{PP}:1L_{PP}] ([0,0,0] located at mid-ship). This implies that only a half hull is modelled with a symmetry boundary condition at y = 0. For the double-body model the free surface is represented by a horizontal plane with symmetry boundary condition located at z = 0. For the free surface model, the surface is modeled using the Volume-of-fluid (VOF) method, with the convective term discretized using the High Resolution Interface Capturing (HRIC) scheme. Further, for the free surface model the heave and pitch motions are modeled with the DFBI Equilibrium model in STAR-CCM+, implying that the model moves the body stepwise to obtain balanced forces and moments without solving the equations of motions. The double-body models are locked in the position obtained in the free-surface models. A fixed inlet velocity boundary condition is specified at the inlet and lateral boundaries. On the outlet, a hydrostatic pressure is prescribed for the free surface setup, where gravity is accounted for, and a uniform static pressure for the double-body model. The time step is set so it on average takes 200 time steps for a fluid particle to pass the hull.

The model-scale hull is modelled as a smooth wall, except the area covered with a sandpaper-stripe. To ensure turbulent boundary layers downstream of the sandpaper-stripe when employing the $\gamma - Re_\theta$ transition model, this surface is modelled as rough, using the default roughness model implemented in STAR-CCM+ for low-Reynolds number turbulence models [4] and an equivalent sand grain roughness (k_s) of 300 μm. This roughness height was found appropriate to trigger turbulence, but it is not investigated to which extent it is a correct physical representation of the sandpaper-stripe. In ship-scale the hull is modelled as a rough wall. It is assumed that the roughness can be modelled using a Colebrook/Grigson-type of roughness-function, $\Delta U^+ = 1/\kappa \cdot \ln(1 + k^+)$ with $k_s = 27$ μm. The value is estimated based on reverse engineering to approximately replicate test-institute ship-scale predictions.

For the self-propulsion setups the propeller rotation is simulated applying sliding meshes with a time step corresponding to 1° propeller rotation. The rotation rates are adjusted to meet desired difference between propeller thrust and hull resistance. In model-scale, a representative experimental tow force adjusted for the estimated wave-making resistance is applied. In ship-scale, equilibrium is assumed and hence the difference aimed for is the ship-scale estimated wave-making resistance.

2.3 Computational Grids

In model-scale the boundary layers are resolved down to the wall, while in ship-scale wall functions are applied to model the boundary layers. In model scale, the propeller boundary layers are resolved using an expansion ratio of 1.1 and average $y^+ < 0.4$, see Figure 3 for a sectional cut of the model-scale propeller grid, focusing on the leading edge. In ship-scale, the resulting y^+ is in average 60. Grid sensitivity analyses of the propeller grid in model-scale show that a refined grid with cell sizes about 25% smaller than the applied grid (total propeller domain cell count increased with about 60%) predicts 0.1% higher efficiency at J = 0.7. Numerical errors of that order of magnitude are considered acceptable, considering that grid convergence when applying

a transition model is more difficult, and refining the grid further would imply an unacceptable computational cost.
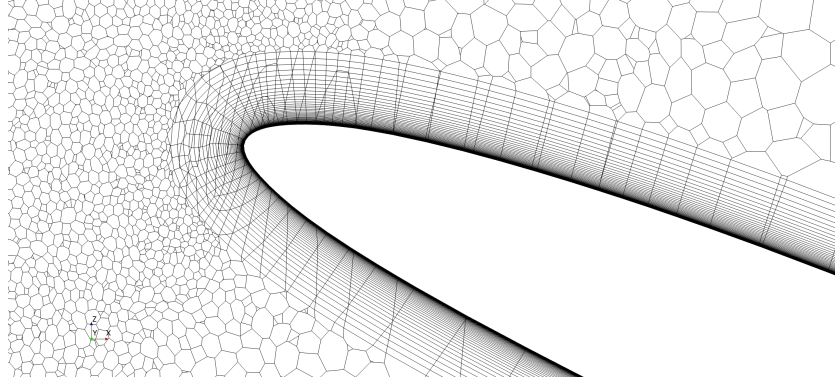

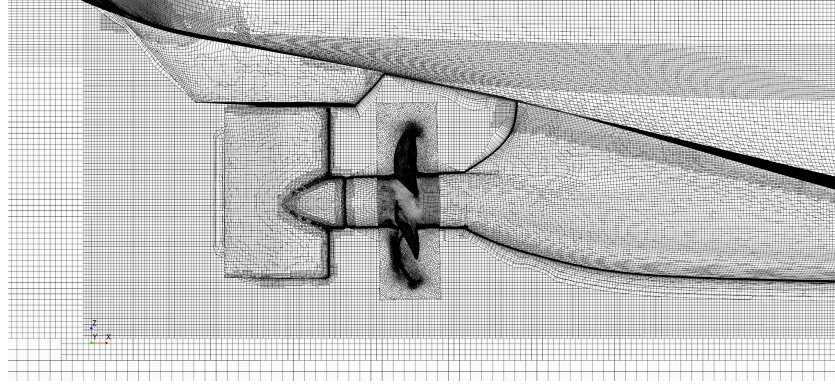**Figure 3**: Sectional cut $(0.7D_P)$ of model-scale propeller grid

Figure 4: Sectional cut and wall-surface grid in the propulsion system region

Table 2: Cell count for computational grids

	Model-scale	Ship-scale
Propeller	$18.9 \cdot 10^6$	$9.6 \cdot 10^6$
Open Water, outer domain	$2.5 \cdot 10^6$	$2.5 \cdot 10^6$
Bare hull, free surface	$24.4 \cdot 10^6$	$21.2 \cdot 10^6$
Bare hull, double-body model	$18.2 \cdot 10^6$	$15.6 \cdot 10^6$
Self-propulsion outer domain, double-body model	$18.1 \cdot 10^6$	$15.5 \cdot 10^6$

On the hull, the average y^+ is 0.25 and 200 in model and ship-scale, respectively. Apart from the prism layers, identical grid parameter settings are applied for model and ship-scale. Volumetric refinements are used around bow and stern, and for the free surface simulations

anisotropic cell refinements are used around the free surface. Grid sensitivity analyses are conducted for the bare hull double-body model in model-scale and show a minor ($<$0.1%) influence on resistance with a refined grid (all targeted sizes reduced by 25%). An additional grid sensitivity analysis was also conducted for the self-propulsion case, where the cell size of the refinement region around the propulsion system was reduced by a factor of 2; this had a negligible influence ($<$0.2%) on the overall variables. The grid (sectional cut and wall-surface grid) in the region surrounding the propulsion system is shown in Figure 4. Table 2 summarizes the number of cells for each domain.

3 RESULTS

The ship-scale results indicate 1.2% less power requirements in-behind for the conventional in relation to the ice classed propeller. From Table 3 it is clear that this is due to a reduced rotation rate at the same time as the torque increases slightly. This difference is less than what is expected based on the open water efficiencies. The difference in η_O between the propellers at J = 0.725 (similar to the time-averaged advance ratio in-behind) is about 1.5%, and η_O evaluated using K_T-identity, which also is influenced by system performance, differs 2.4%, as listed in Table 3. So the question to be answered is why the conventional propeller is less efficient in behind compared to what is expected based on open water performance. As also seen from Table 3, the propellers need to deliver about the same thrust, so differences in thrust deduction is of minor importance.

Table 3: CFD-predicted self-propulsion overall variables and propulsive factors in ship-scale

Propeller	Ice classed	Conventional
n [rpm]	95.59	94.10 (-1.6%)
Thrust [kN]	354.1	353.8 (-0.1%)
K_T	0.1658	0.1709 (3.1%)
Torque [kNm]	278.7	279.6 (0.3%)
K_Q	0.02900	0.03002 (3.5%)
Tow force [kN]	0.10	0.03
Power [kW]	2790	2755 (-1.2%)
t	0.109	0.108 (-0.9%)
w_T	0.225	0.222 (-1.3%)
η_R	1.001	0.993 (-0.8%)
η_O	0.657	0.672 (2.4%)

Figure 5 displays K_T/K_Q for the ship-scale propeller blades around a revolution, a measure of the blade performance in-behind. This measure is naturally influenced by differences in propeller performance in homogeneous inflow, however it is clear that the conventional propeller has a lower K_T/K_Q, i.e. is performing worse, than the ice classed propeller around 270°. This tangential position corresponds to when the blade motion is upwards, aligned with the upwards directed flow around the stern, resulting in a low loaded blade. The same observation can be made also in model-scale, as shown in Figure 6. At this scale, the difference between the propellers is slightly less around 270°, which most probably is due to a combination of the

larger nominal model-scale wake as shown in Figure 7 and issues related to performance at low Reynolds numbers, to be discussed further below.
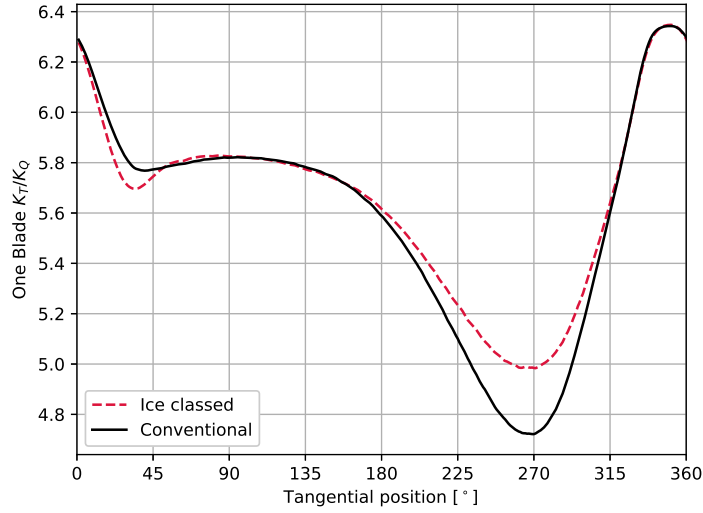

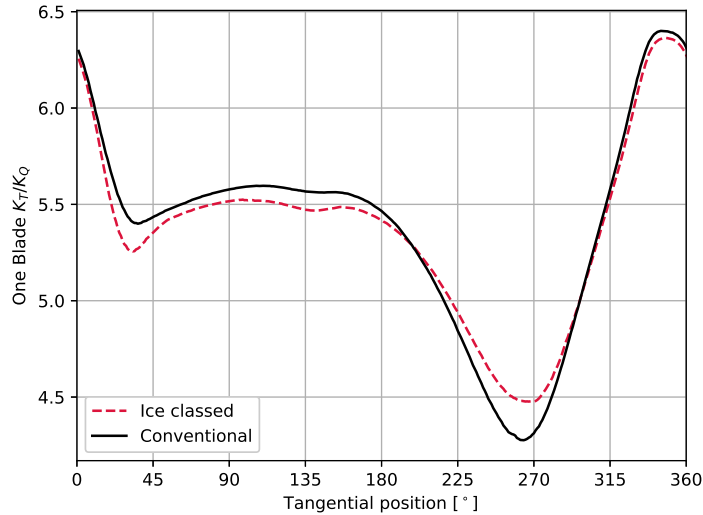**Figure 5**: Ship-Scale CFD results for K_T/K_Q variation in the wake

Figure 6: Model-Scale CFD results for K_T/K_Q variation in the wake

In Figure 8 the radial K_T/K_Q-distributions are evaluated for the blades in the wake at $270°$ as well as in open water. The results are shown in ship-scale, but the same trend is present in
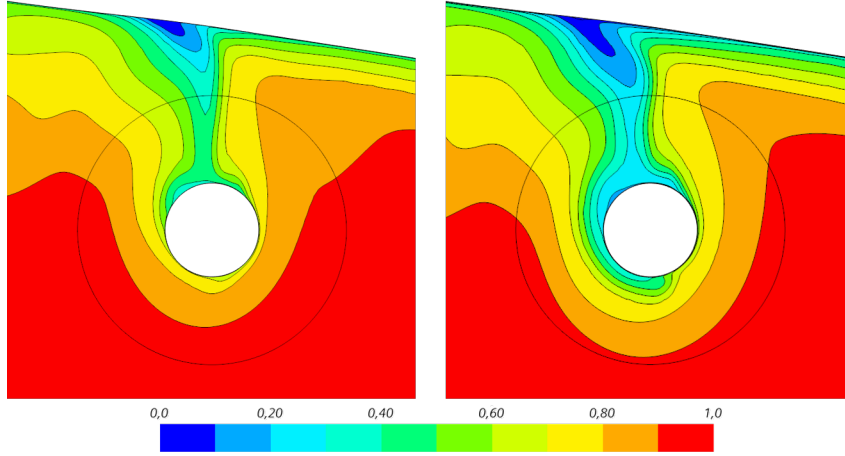
7

Figure 7: Contour plots of nominal axial velocity at propeller plane in ship-scale (left) and model-scale (right)

model-scale. An inferior performance is especially noted towards the tip for the conventional propeller. As expected, and visible in Figure 7, the wake implies lower axial velocities towards the hub and higher towards the tip in relation to open water operation. Hence, around $270°$ the outer blade sections experiences a very low load, and even negative angles of attack, due to a combination of the high axial velocities and blade motion aligned with the upwards directed flow around the stern. The contour plots in Figure 9, shows a radial cut at r/R=0.9 for both propellers at $270°$. At this section the angles of attack are negative, for the conventional propeller the flow cannot follow the sharp leading edge of the profile onto the pressure side, resulting in an even lower pressure on the pressure side. The blunter leading edge of the ice classed propeller is capable of maintaining an attached flow even at this angle of attack. The lower rotation rate of the conventional propeller in-behind is amplifying this effect since it implies lower angles of attack, i.e. more negative. The superior performance of a blunt leading edge at low load can also explain why the efficiency peak of ice classed propeller is noted at higher advance ratio in relation to the conventional propeller, as seen in Figure 10.

The model-scale results are included in Table 4. At this scale factor the delivered power is 1.9% lower for the conventional propeller in relation to the ice classed. This is a larger difference than what is expected from the open water performance of each propeller in model-scale, hence the opposite observation to the ship-scale results. In model-scale, η_O differs about 1.1% at these advance ratios, and η_O evaluated using K_T-identity differs 1.7%. Also for this scale-factor the propellers need to deliver about the same thrust, i.e. similar thrust deduction. The observation made above still holds, i.e. that the ice classed propeller benefits from its blunt profile in-behind since it performs better at low load, even if the effect most probably not is as large due to the larger model-scale wake. However, another effect must be present to counteract the benefits of the ice classed propeller in behind. Our view is that this to the largest extent is explained by differences in performance due to different Reynolds numbers in model-scale open water and self-propulsion tests. In this study, self-propulsion is conducted at Re $\approx$ 200 000 and open water at Re $\approx$ 750 000.
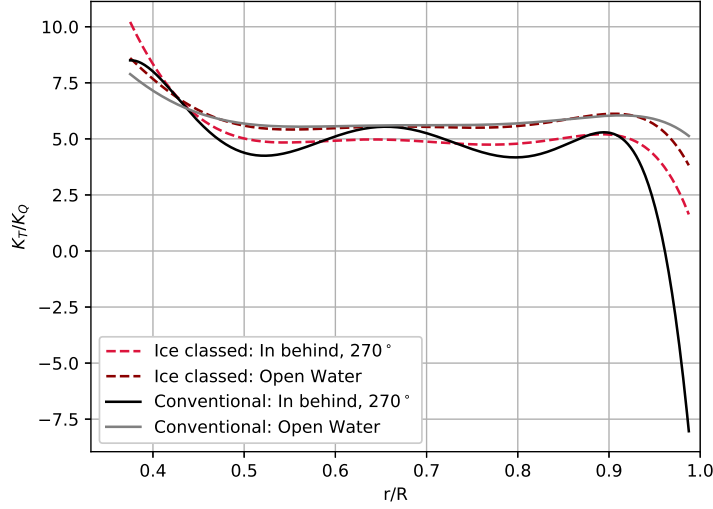
Figure 8: Ship-Scale CFD results for radial variation of K_T/K_Q at the tangential blade position 270°. Open water at self-propulsion average K_T.

Figure 9: Ship-Scale CFD results; contours of velocity magnitude in a reference frame rotating with the propeller at a radial section at r/R = 0.9. Ice classed propeller (top) and conventional propeller (bottom). Contour scale 0-23 m/s.
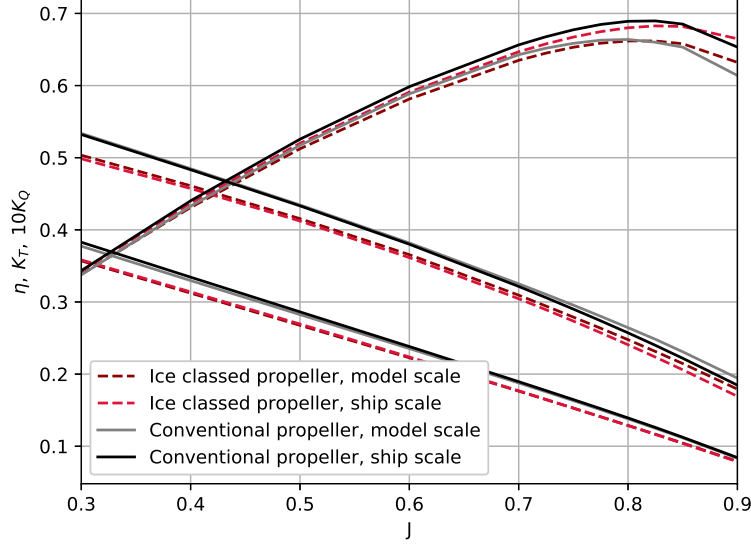
Figure 10: CFD results for the propellers in Open Water

Table 4: CFD-predicted self-propulsion overall variables and propulsive factors in model-scale

Propeller	Ice classed	Conventional
n [rps]	6.9570	6.8674 (-1.3%)
Thrust [N]	36.06	36.08 (+0.1%)
K_T	0.1745	0.1792 (2.7%)
Torque [Nm]	0.7088	0.7043 (-0.6%)
K_Q	0.03190	0.03253 (2.0%)
Tow force [N]	15.12	15.09 (-0.2%)
Power [W]	61.97	60.78 (-1.9%)
t	0.124	0.123 (-0.4%)
w_T	0.278	0.275 (-1.0%)
η_R	0.962	0.968 (0.7%)
η_O	0.638	0.649 (1.7%)

In Figure 11, η_O is evaluated at J = 0.725, which is close to the self-propulsion average loading, for four different Reynolds numbers. The efficiency of the conventional propeller reduces less with reduced Reynolds number compared to the ice classed propeller. Studying the flow in more detail it is noted that the thicker profiles of the ice classed propeller are punished to a higher degree by the thicker boundary layers at lower Reynolds numbers. The differences are noted towards the trailing edge where a thicker profile is more prone to separation at low Reynolds numbers. That a thicker profile implies higher scale effects on K_T and K_Q is also incorporated in the common ITTC-78 scaling procedure for open water characteristics from model to ship-scale[1].
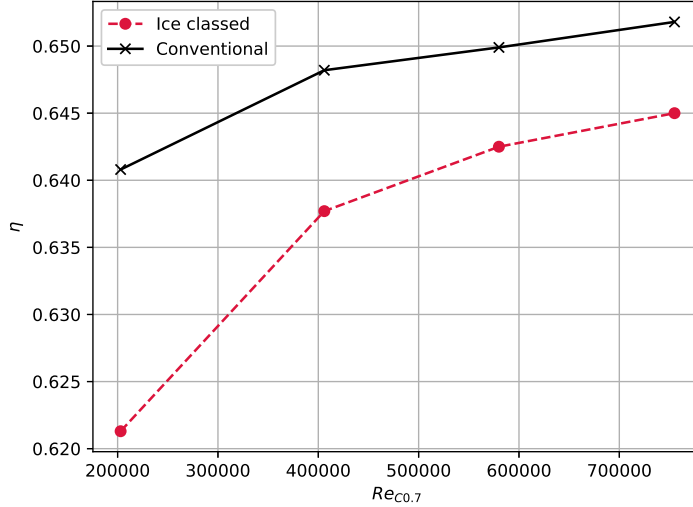
10

Figure 11: Model-Scale CFD results; propeller open water efficiency versus Reynolds number

4   CONCLUSIONS

In ship-scale, the performance degradation of an ice classed propeller in-behind is less than in open water due to superior performance at very low load; it is less sensitive to negative angles of attack. This is also the reason why the open water efficiency peak of the ice classed propeller is noted at higher advance ratios. This effect is most probably less in model-scale self-propulsion due to a larger wake. Secondly, in model-scale self-propulsion the ice classed propeller is punished by the low Reynolds number of the test; the blunter profile suffers more at lower Reynolds numbers, which counteracts the benefits of better performance at low load. Both these observations clearly illustrates how the model-scale wake, as well as the low Reynolds number of the self-propulsion test can influence the propulsion system performance, and hence propulsive factors, differently for different propulsion systems.

5   ACKNOWLEDGEMENTS

REFERENCES

[1] ITTC. 1978 ITTC Performance Prediction Method. Recommended Procedure 7.5 - 02 - 03 - 01.4 Rev 04, 2017.

[2] Thomas Lücke. Particular Model Propeller Behavior in EFD & CFD. In *Proceedings of the Sixth International Symposium on Marine Propulsors*, Rome, Italy, 2019.

[3] Da-Qing Li, Per Lindell, and Sofia Werner. Transitional flow on model scale propellers and their likely influence on performance prediction. In *Proceedings of the Sixth International Symposium on Marine Propulsors*, Rome, Italy, 2019.

[4] Siemens PLM Software. STAR-CCM+ Documentation version 2019.3, 2019.

[5] F. R. Menter. Two-equation eddy-viscosity turbulence models for engineering applications. *AIAA Journal*, 32(8):1598–1605, 1994.

[6] F. R. Menter, M. Kuntz, and R. Langtry. Ten Years of Industrial Experience with the SST Turbulence Model. In K Hanjalic, Y Nagano, and M Tummers, editors, *Turbulence, Heat and Mass Transfer 4*. Begell House, Inc., 2003.

[7] P. R. Spalart. Strategies for turbulence modelling and simulations. *International Journal of Heat and Fluid Flow*, 21(3):252–263, 2000.

[8] Sunil K. Arolla and Paul A. Durbin. Modeling rotation and curvature effects within scalar eddy viscosity model framework. *International Journal of Heat and Fluid Flow*, 39:78–89, 2013.

[9] R. B. Langtry, F. R. Menter, S. R. Likki, Y. B. Suzen, P. G. Huang, and S. Volker. A Correlation-Based Transition Model Using Local Variables Part II: Test Cases and Industrial Applications. *Journal of Turbomachinery*, 128(3):423, 2006.

[10] F R Menter, R B Langtry, S R Likki, Y B Suzen, P G Huang, and S Völker. A Correlation-Based Transition Model Using Local Variables Part I: Model Formulation. *Journal of Turbomachinery*, 128(3):413–422, 2004.

[11] Robin B. Langtry, Kaustav Sengupta, David T. Yeh, and Andrew J. Dorgan. Extending the γ-Reθt Local Correlation based Transition Model for Crossflow Effects. In *45th AIAA Fluid Dynamics Conference*, pages 1–12, Dallas, USA, 2015.